Geophysical Research Letters

RESEARCH LETTER
10.1029/2019GL086592

Climate Models and Remote Sensing Retrievals Neglect Substantial Desert Dust Asphericity

Yue Huang[1], Jasper F. Kok[1], Konrad Kandler[2], Hannakaisa Lindqvist[3], Timo Nousiainen[3], Tetsu Sakai[4], Adeyemi Adebiyi[1], and Olli Jokinen[5]

[1]Department of Atmospheric and Oceanic Sciences, University of California, Los Angeles, CA, USA, [2]Institute for Applied Geosciences, Technical University Darmstadt, Darmstadt, Germany, [3]Finnish Meteorological Institute, Helsinki, Finland, [4]Meteorological Research Institute, Japan Meteorological Agency, Tsukuba, Japan, [5]Sole Proprietorship, Espoo, Finland

Abstract Climate models and remote sensing retrievals generally assume that dust aerosols are spherical or spheroidal. However, measurements show that dust aerosols deviate substantially from spherical and spheroidal shapes, as ratios of particle length to width (the aspect ratio) and height to width (height-to-width ratio) deviate substantially from unity. Here, we quantify dust asphericity by compiling dozens of measurements of aspect ratio and height-to-width ratio across the globe. We find that the length is on average 5 times larger than the height and that climate models and remote sensing retrievals underestimate this asphericity by a factor of ~3–5. Compiled measurements further suggest that North African dust becomes more aspherical during transport, whereas Asian dust might become less aspherical. We obtain globally-averaged shape distributions, from which we find that accounting for dust asphericity increases gravitational settling lifetime by ~20%. This increased lifetime helps explain the underestimation of coarse dust transport by models.

Key Points:
- A compilation of measurements shows that current climate models and remote sensing retrievals substantially underestimate dust asphericity
- Measurements suggest that North African dust becomes more aspherical during transport, whereas Asian dust might become less aspherical
- Dust asphericity increases gravitational settling lifetime by ~20%, which helps explain the underestimation of coarse dust transport by models

Supporting Information:
- Supporting Information S1

Correspondence to:
Y. Huang,
hyue4@ucla.edu

Citation:
Huang, Y., Kok, J. F., Kandler, K., Lindqvist, H., Nousiainen, T., Sakai, T., et al. (2020). Climate models and remote sensing retrievals neglect substantial desert dust asphericity. *Geophysical Research Letters*, *47*, e2019GL086592. https://doi.org/10.1029/2019GL086592

Received 7 DEC 2019
Accepted 24 FEB 2020
Accepted article online 11 MAR 2020

1. Introduction

Desert dust is the dominant aerosol type by mass in the atmosphere (Boucher et al., 2013). It produces important effects on the Earth system, including by directly modulating the radiation budget (Kok et al., 2017; Pérez et al., 2006), modifying cloud microphysics (DeMott et al., 2003), catalyzing heterogeneous chemistry (Usher et al., 2002), and fertilizing ecosystems (Jickells et al., 2005). Furthermore, dust aerosols affect regional air quality (Huang et al., 2019; Mahowald et al., 2007), producing hazards to human health (Burnett et al., 2014). These varied impacts depend on the optical and aerodynamical properties of desert dust. Because the optical and aerodynamic properties of aspherical dust differ significantly from volume-equivalent spherical dust (Nousiainen & Kandler, 2015; Yang et al., 2013), dust impacts are sensitive to the shape of dust aerosols.

Although an accurate quantification of dust shape is thus important for calculating dust impacts, current representations of dust shape in climate models and remote sensing retrievals conflict with *in situ* measurements. Most current climate models approximate dust aerosols as spherical particles (Figure S1a in the supporting information) (Mahowald et al., 2014), while retrieval algorithms of passive remote sensing instruments approximate dust as spherical or spheroidal particles (Figures S1b and S1c). For example, the Version 2 and Version 3 inversion algorithms of the ground-based Aerosol Robotic Network (AERONET) use precomputed lookup tables of the single-scattering properties of spheroidal dust to retrieve dust properties (Dubovik et al., 2006). A second example is the Version 23 operational retrieval algorithm of the satellite-borne Multiangle Imaging Spectroradiometer (MISR), which approximates coarse-mode dust as spheroids, medium-mode dust as cubic blocks, and fine-mode dust as spheres (Kalashnikova et al., 2005). That is, climate models and remote sensing retrievals assume that either all three or two of the three dimensions of dust aerosols are equal (Figure S1). However, several *in situ* measurements have shown that the ratios of dust length to its width and dust height to its width deviate substantially from unity (e.g., Okada et al., 2001). As such, both climate models and remote sensing retrievals likely underestimate dust asphericity by assuming that at least two of the three dimensions are equal. This possible bias in climate models and remote sensing retrievals can propagate into calculations of dust impacts. For instance, as dust asphericity slows gravitational settling by increasing aerodynamic drag at a given volume and mass (Yang et al., 2013), this bias toward spherical dust might have caused an underestimation of dust dry lifetime.

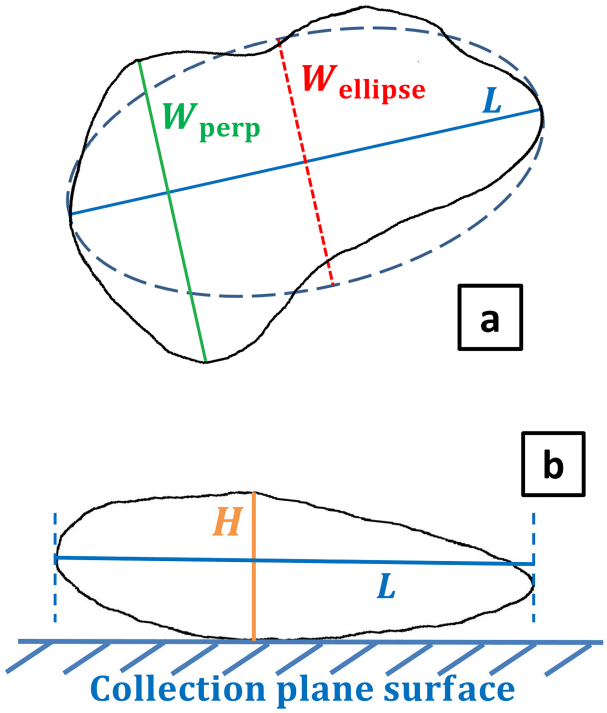

Figure 1. (a) Top view of two-dimensional (2-D) projected area (within the black line) of a dust particle and (b) side view, along the length L (blue line) defined in (a), of the same particle collected on a plane surface by impactors. Panel (a) demonstrates the systematic difference in the two common quantifications of dust width. The first definition records the maximum distance between two points on the outline that is perpendicular to the length L as the width W_{perp} (green line). The second definition records the width $W_{ellipse}$ (red dashed line) as the minor axis of an area-equivalent ellipse (blue dashed line) with L as its major axis. Because W_{perp} is systematically larger than $W_{ellipse}$ (Table S1 and Figure S2), this systematic difference causes a systematic bias between experimental studies using different definitions of particle width. Panel (b) demonstrates the definition of dust height. The height H (orange line) is defined as the maximum distance between the outline of the particle to the collection surface that is perpendicular to the collection surface.

To facilitate accounting for dust asphericity in climate models and remote sensing retrievals, here we compile dozens of measurements of dust shape across the globe. To do so, we first introduce the shape descriptors that we use to quantify dust asphericity in section 2. In section 3, we then present the compiled results of the shape descriptors, globally and regionally. In section 4, we use our compiled shape distributions to quantify the enhancement of gravitational settling lifetime due to dust asphericity. Our results show that dust asphericity has been substantially underestimated by climate models and remote sensing retrievals, which helps explain the underestimation of coarse dust transport by climate models.

2. The Shape Descriptors of Aspherical Dust

The most widely used descriptors to quantify dust asphericity are the aspect ratio (AR) and the height-to-width ratio (HWR), which are less sensitive to microscopic image resolution and artifacts than other shape descriptors (Almeida-Prieto et al., 2007; Kandler et al., 2011). In remote sensing retrievals, AR is the ratio of a particle's length to its height (e.g., Dubovik et al., 2006), whereas HWR is normally not used as dust particles are normally approximated as spheroids (Figure S1). However, in *in situ* measurements, the AR is usually taken as the ratio of the largest dimension of a particle's projected area (the length) to the perpendicular dimension of the projected area (the width; see Figure 1a). Further, the height is usually taken as the dimension perpendicular to the collection surface (the height; see Figure 1b). Because most impactor-collected dust particles deposit with their smallest dimension perpendicular to the collection surface, the HWR usually equals a particle's smallest dimension (the height) divided by the smaller dimension on the projected area (the width) (Okada et al., 2001; Sakai et al., 2010).

2.1. Measurements of the Aspect Ratio and the Height-to-width Ratio

To quantify AR, many studies have measured the particle length and width of two-dimensional (2-D) scanning electron microscopic (SEM) images of individual dust particles (e.g., E.A. Reid et al., 2003). Specifically, individual dust aerosols are usually collected on filters by ground-based or aircraft-carried impactors (e.g., Kandler et al., 2007), after which 2-D top view SEM images of the collected particles were obtained. These 2-D images were then analyzed to obtain the length and width of individual dust particles (e.g., Kandler et al., 2007). The length L is usually taken as the longest distance between two points on the outline of the projected area (Figure 1a). Although the length is usually defined consistently between measurements (e.g.,Okada et al., 2001 ; Sakai et al., 2010), a systematic difference exists between the two common definitions of the width. Some studies obtained the width W_{perp} as the maximum distance that is perpendicular to L (Figure 1a) (e.g., Okada et al., 2001). In contrast, other studies obtained the width $W_{ellipse}$ as the minor axis of an ellipse with an area equal to that of the particle's projected area and with L as its major axis (Figure 1a) (e.g., Kandler et al., 2007). In this latter case, studies have found that the ratio of the two dimensions of the projected area (i.e., AR) follows a modified lognormal distribution (e.g., Kandler et al., 2007),

$$f(AR) = \frac{1}{\sqrt{2\pi}\cdot(AR-1)\cdot\sigma_a} exp\left[-\frac{1}{2}\left(\frac{ln(AR-1)-ln(\overline{\varepsilon_a}-1)}{\sigma_a}\right)^2\right], \quad (1)$$

where σ_a is the geometric standard deviation of the deviation of AR from unity (AR-1) and $\overline{\varepsilon_a}$ is the median of AR.

A subset of studies that measured AR also measured the dust height, the dimension of the particle perpendicular to the collection plane surface (see Figure 1b and supporting information Text S1). Those studies that

obtained extensive data sets (Okada et al., 2001; Osada, 2013; Sakai et al., 2010) have found that the ratio of the height to the width (i.e., HWR) follows a lognormal distribution

$$f(HWR) = \frac{1}{\sqrt{2\pi}\cdot HWR\cdot\sigma_h} exp\left[-\frac{1}{2}\left(\frac{ln(HWR)-ln(\overline{\varepsilon_h})}{\sigma_h}\right)^2\right], \quad (2)$$

where σ_h and $\overline{\varepsilon_h}$ are, respectively, the geometric standard deviation and median of HWR.

2.2. Addressing the Systematic Difference in Particle Width

Measurements of AR and HWR are affected by the systematic difference in the two common definitions of the particle width. We address this systematic difference between measurements of W_{perp} and $W_{ellipse}$ using shape measurements of 13 dust particles collected from the Saharan Mineral Dust Experiment campaign (SAMUM; Lindqvist et al., 2014) and two dust particles collected from the African Monsoon Multidisciplinary Analyses campaign (AMMA; Chou et al., 2008). For each of the 15 particles, we computed W_{perp} and $W_{ellipse}$ and found that the average correction factor ($c = \frac{W_{perp}-W_{ellipse}}{W_{ellipse}}$) is 13.7 % $\pm$ 2.7% (Table S1). Because of the small number of dust particles, we further calculated the correction factors of 1,261 African and 681 Asian laboratory-generated dust particles (Sakai et al., 2010), for which the average correction factor is 27.2 % $\pm$ 0.4% for all 1,941 dust particles (Figure S2). This correction factor is larger than that of the 15 SAMUM and AMMA dust particles, due to unknown dependences of the correction factor on the physical and chemical properties (such as particle size, mineralogy, and morphology). Although the representativeness of laboratory-generated dust particles is unclear, because of its extensive number of sampled dust particles, we took $c = 20\ \% \pm 6\%$ as the approximate average of the two data sets with a large uncertainty range that covers both data sets. We thus linked W_{perp} and $W_{ellipse}$ by

$$W_{ellipse} = \frac{W_{perp}}{1+c} \quad (3)$$

3. Measurement Compilation of Dust Shape Descriptors

We compiled dozens of measurements of AR and HWR of dust aerosols across the globe (see the map of measurement sites in Figure S3). Specifically, for each measurement, we first found the published medians of AR and HWR (Column 8 of Tables S2 and S3) and applied equation (3) to correct all medians that used W_{perp} instead of $W_{ellipse}$ (Column 10 of Tables S2 and S3). We correct W_{perp} to $W_{ellipse}$ because $W_{ellipse}$ quantifies the particle's projected area, which is strongly linked to its aerodynamic and optical properties (Mahowald et al., 2014). Second, we obtained the geometric standard deviations of AR-1 and HWR by fitting lognormal distributions (equations (1) and (2)) to data of the probability functions of AR ($=L/W_{ellipse}$) and HWR ($=H/W_{ellipse}$), corrected to $W_{ellipse}$ if needed. These lognormal fits used the median AR and HWR obtained from Step 1. Third, we grouped the medians and geometric standard deviations by source regions (Asian or North African sources) and transport distance (source, short-range transport, or long-range transport). Finally, we averaged all medians and geometric standard deviations to obtain the globally-averaged shape distributions of AR and HWR of dust aerosols. Although our methodology is subject to a few limitations (see section 5), our compilation yields a number of key findings.

First, dust shape shows little dependence on particle diameter in the range of 0.1–20 μm (Figure 2). Although some individual measurements find a dependence of AR on dust diameter (e.g., Kandler et al., 2007; E.A. Reid et al., 2003), a regression with all available data shows that AR is proportional to dust diameter with a small exponent of 0.011 $\pm$ 0.010, which is statistically not different from zero. Although the HWR decreases more substantially with dust size, with a power law exponent of -0.06 ± 0.35, this dependence is not statistically significant. The ratio of dust length to its height (LHR; Figure 2e), obtained by combining AR and HWR, increases somewhat with dust diameter, but this increase is also not statistically significant, with a power law exponent of 0.04 $\pm$ 0.36.

Second, the dependence of AR on source region is less than thought. We find that the averaged median AR of North African dust is 1.72 $\pm$ 0.02 and that of Asian dust is 1.60 $\pm$ 0.08. Although the AR of North African dust might thus be larger than that of Asian dust (p value = 0.001 from Student's t test), this regional difference is

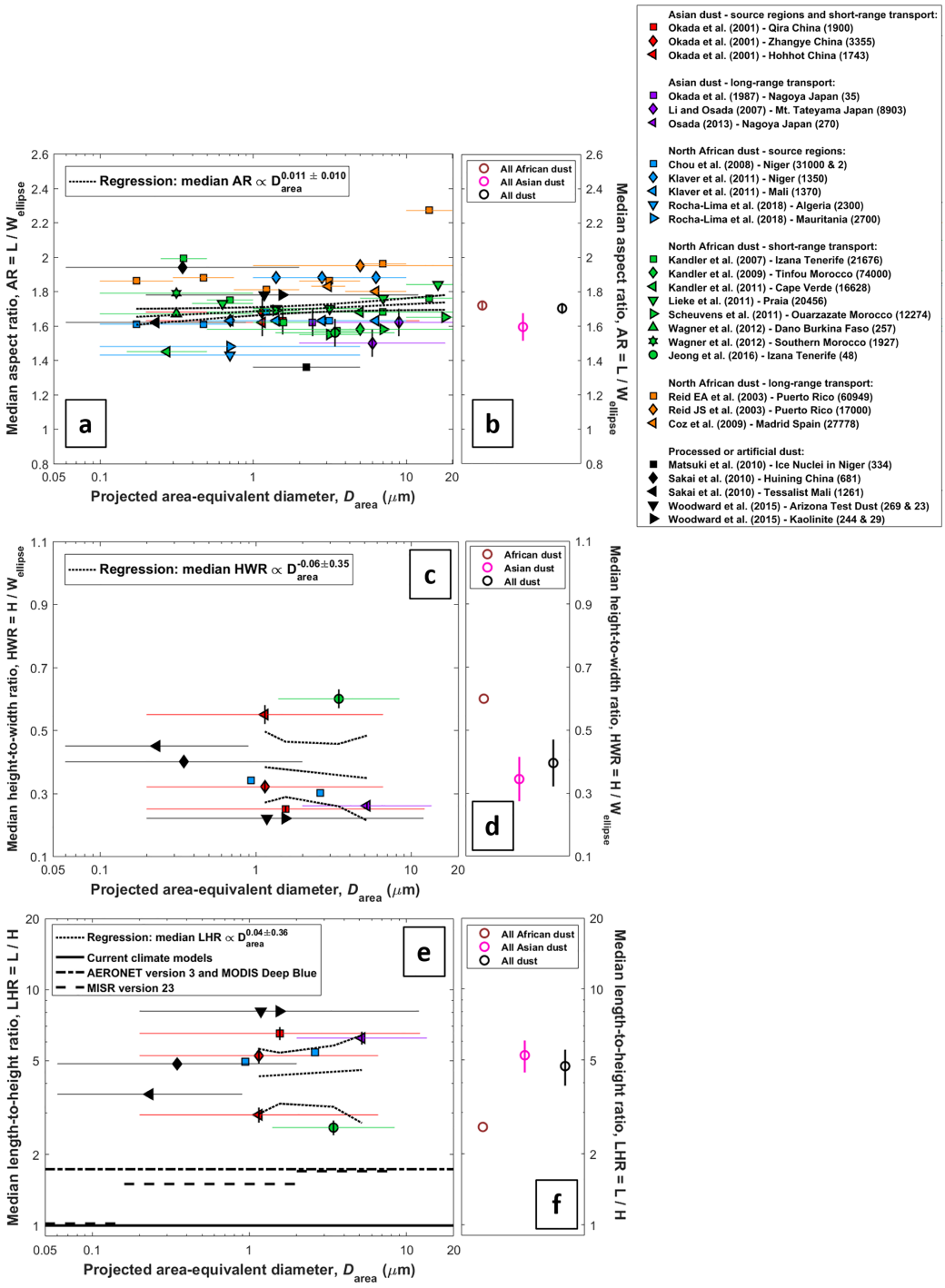

Figure 2. Measurement compilation of the medians of (a) the aspect ratio, (c) the height-to-width ratio, and (e) the length-to-height ratio as a function of projected area-equivalent diameter. The horizontal bars in (a), (c), and (e) show the bin ranges of the measurements, and the markers are plotted on the geometric means of the size ranges. The vertical bars in (a) and (c) denote errors from the uncertainty of the correction factor, and the vertical bars in (e) denote errors that propagate from (a) and (c). In the legend, the numbers in parentheses denote the numbers of analyzed individual dust particles. Chou et al. (2008) and Woodward et al. (2015) have two numbers with the first one denoting the number of analyzed dust particles for AR and the second one for HWR. In (c) and (e), Chou et al. (2008) is not used in regressions due to the insignificant number of analyzed particles for HWR. In (e), values of the ratio of dust length to its height for climate models and retrieval algorithms are based on Mahowald et al. (2014), Dubovik et al. (2006), Hsu et al. (2019), and Kalashnikova and Kahn (2006), respectively. MISR v23 is unity for diameter <0.16 μm and offset for clarity. Results grouped by source regions are shown in (b), (d), and (f). The vertical uncertainty ranges in (b), (d), and (f) denote the propagated error in the median. In (d) and (f), the errors of African dust are not shown due to only one measurement of HWR (Jeong et al., 2016). Results of measurements of processed or artificial dust (Matsuki et al., 2010; Sakai et al., 2010; Woodward et al., 2015) are shown for completeness, but because their representativeness to real mineral dust aerosols is unclear, these studies are not used in the groupings in (b), (d), and (f) or in regressions in (a), (c), and (e).

much less than concluded in previous studies (e.g., Formenti et al., 2011; Li & Osada, 2007) due to the systematic difference in the definition of particle width (Figure 1a). Specifically, measurements of Asian dust have quantified AR and HWR in terms of W_{perp} (e.g., Li & Osada, 2007), whereas measurements of North African dust have generally used $W_{ellipse}$ (e.g, E.A. Ried et al., 2003) (see Tables S2 and S3). Since W_{perp} is systematically larger than $W_{ellipse}$ (Table S1 and Figure S2), this has caused measurements of Asian dust to report a smaller AR than measurements of North African dust. Furthermore, the averaged median HWR of North African dust is 0.60 and that of Asian dust is 0.35 ± 0.07. Although this difference is statistically significant (p value = 0.04), it is uncertain due to a scarcity of measurements of HWR, especially for North African dust, for which only one measurement has been published (Jeong et al., 2016).

Third, North African dust becomes more aspherical during transport, whereas Asian dust may become less aspherical (Figure 3). For North African dust, the median of AR increases from 1.60 ± 0.07 in source regions to 1.66 ± 0.03 for short-range transported dust and 1.90 ± 0.04 for long-range transported dust. The differences between source regions and long-range transported dust (p value = 0.001) and between short- and long-range transported dust (p value = 0.002) are statistically significant. Our finding that the median of North African AR increases substantially during transport agrees with previous studies (e.g., Coz et al., 2009; Formenti et al., 2011). This increase in particle asphericity during transport is likely due to the preferential settling of spherical particles, which have a greater terminal fall speed than aspherical particles of the same volume (Yang et al., 2013). In contrast to this increase in dust asphericity during transport of North African dust, we find that the median AR of Asian dust decreases during transport from 1.64 ± 0.07 in source regions and short-range transported dust to 1.58 ± 0.05 for long-range transported dust. Although this difference is not significant at the 5% level (p value = 0.25), this finding indicates that, for Asian dust, a second mechanism offsets the increase in asphericity due to preferential settling of spherical particles during transport. In particular, chemical processing with sea salts and humic acids can form a uniform coating around the mineral core and therefore decrease particle asphericity during transport (Alexander et al., 2015; Laskina et al., 2013; Zhang, 2008). This process seems substantially more important for Asian than for North African dust (Denjean et al., 2015). Furthermore, the medians of AR close to source region are statistically not distinguishable between North African and Asian dust (Figures 3b and 3d). This enables a simple shape distribution of dust in source regions.

Finally, both climate models and remote sensing retrievals substantially underestimate dust asphericity by overestimating the ratio of dust height to its length. The globally-averaged medians of AR and HWR are 1.70 ± 0.03 and 0.40 ± 0.07 (Figure 2), such that a dust aerosol's length is on average 5 times greater than its height (Figure 2f). In contrast, climate models and remote sensing retrievals assume that dust is spherical or spheroidal, thereby equating at least two of the three dimensions. As a consequence, climate models and remote sensing retrievals underestimate dust asphericity by a factor of ~3–5 (Figure 2e).

4. Lifetime Enhancement Due to Dust Asphericity

The substantial underestimation of dust asphericity by climate models and remote sensing retrievals could produce important errors in determining the impacts of dust on the Earth system. The compiled globally-averaged shape distributions of AR and HWR in Figures 2 and 3 can thus be used to more accurately calculate dust impacts, such as through improved estimates of dust lifetime, optics, and effects on clouds and heterogeneous chemistry. Here, we quantify the effect of dust asphericity on the gravitational settling lifetime of dust, which is neglected in most current climate models (Mahowald et al., 2014).

Gravitational settling of dust aerosols occurs in the Stokes regime as the Reynolds number is far less than 1 (Kok et al., 2012). In the Stokes regime, the terminal velocity of a spherical particle is (e.g., Hinds, 1999)

$$v_{sph} = \frac{g\rho_p}{18\mu} \cdot D^2, \tag{4}$$

where g is the gravitational acceleration, $\rho_p \approx 2.5 \times 10^3$ kg m^{-3} is the typical density of dust aerosols (Kok et al., 2017), $\mu \approx 1.81 \times 10^{-5}$ Pa · s is the dynamic viscosity of air, and D is the diameter of the spherical particle. In analogy to equation (4), we express the terminal velocity of an aspherical particle as follows:

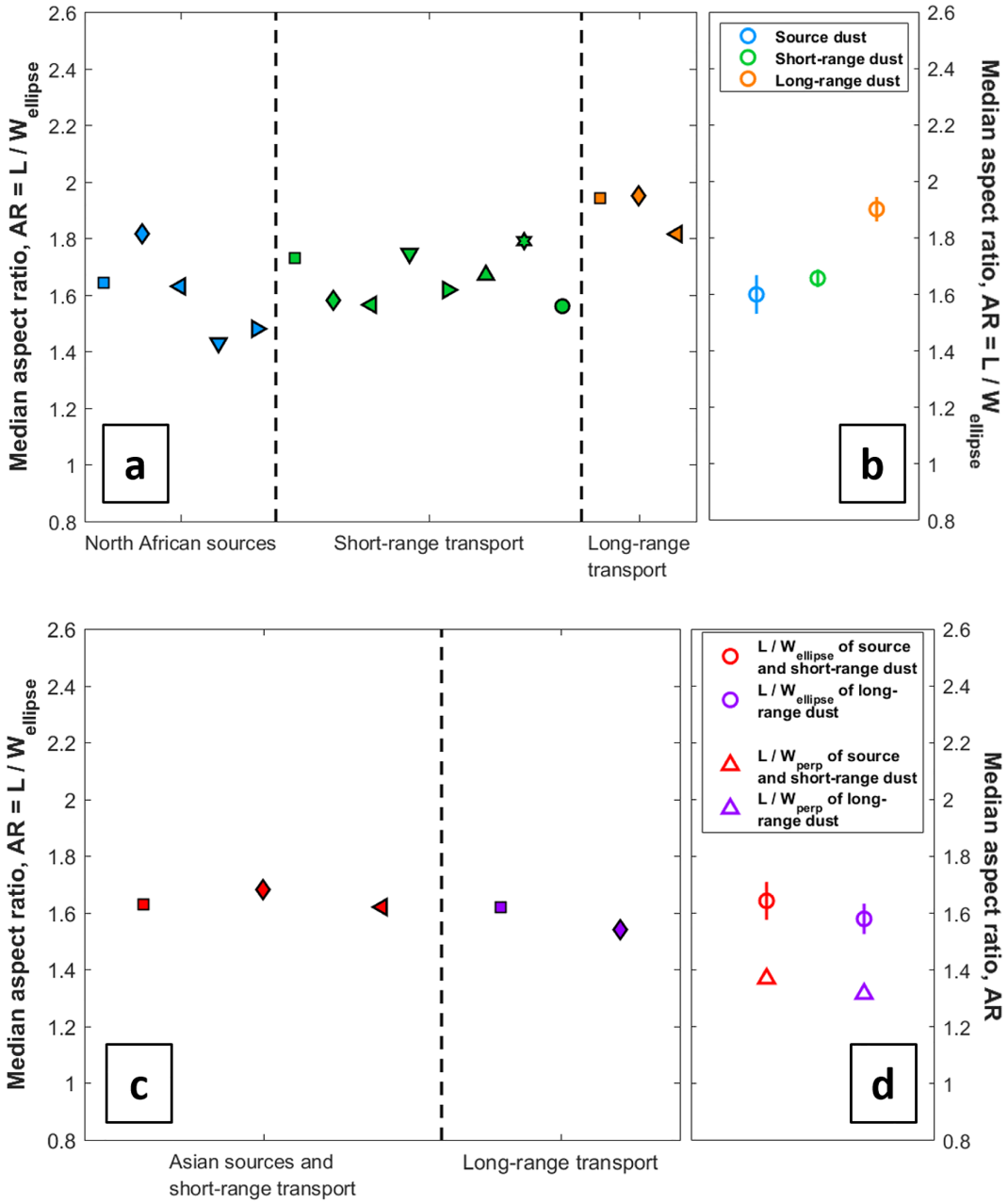

Figure 3. Changes during transport of the median aspect ratio of (a) North African dust and (c) Asian dust. The markers in (a) and (c) are defined in the legend of Figure 2. Results grouped by transport distance (see Figure S3) are shown in (b) and (d). The vertical uncertainty ranges in (b) and (d) denote the propagated error of the median. In (d), median aspect ratios before ($\frac{L}{W_{perp}}$) and after ($\frac{L}{W_{ellipse}}$) the correction of the particle width are shown. This correction leads to a systematic change in all Asian dust studies and therefore does not affect the trend in shape during transport. In the groupings, we used the seasonally-resolved source regions obtained in Ginoux et al. (2012) to distinguish dust in source regions (including Chou et al., 2008; Klaver et al., 2011; Rocha-Lima et al., 2018; Okada et al., 2001 - Qira; Okada et al., 2001 - Zhangye) from transported dust; we then distinguished long-range transported dust (including E.A. Reid et al., 2003; J.S. Reid et al., 2003; Coz et al., 2009; Okada et al., 1987; Li and Osada, 2007) from short-range transported dust (including Kandler et al., 2007; Kandler et al., 2009; Kandler et al., 2011; Lieke et al., 2011; Scheuvens et al., 2011; Wagner et al., 2012; Jeong et al., 2016; Okada et al., 2001 - Hohhot) based on the attributions in publications that reported these measurements. Note that there is not enough data to assess changes of HWR during transport (see Figure S4).

$$v_{asp} = \gamma \frac{g\rho_p}{18\mu} \cdot {D_g}^2, \tag{5}$$

where D_g is the volume-equivalent (geometric) diameter and $\gamma = \frac{v_{asp}}{v_{sph}}$ is the asphericity factor, which equals unity for spherical particles and decreases with increasing particle asphericity at a given volume. To obtain γ,

we use a recent study (Bagheri & Bonadonna, 2016) to quantify γ as a function of the three dimensions of tri-axial ellipsoidal particles (L,W, and H; Figure S1d). This study uses extensive measurements and numerical simulations in the Stokes regime and finds (see their equations (13), (24), and (25))

$$\frac{v_{sph}}{v_{asp}} \equiv k_s = \frac{1}{2}\left({F_s}^{1/3} + \frac{1}{{F_s}^{1/3}}\right), \tag{6}$$

$$F_s = \frac{{D_g}^3}{L^{2.3}.W^{0.7}}, \tag{7}$$

where $D_g = \sqrt[3]{LWH}$. The parameter F_s can be expressed as $HWR{\cdot}\left(\frac{1}{AR}\right)^{1.3}$; $F_s = 1$ for spherical particles and decreases as dust asphericity increases (i.e., an increase of AR and/or decrease of HWR). By combining equations (5)–(7), we obtained the terminal velocity of ellipsoidal particles as a function of its three dimensions.

We used the globally-averaged shape distributions of AR and HWR of dust aerosols to obtain the enhancement of gravitational settling lifetime due to dust asphericity (Figure 4). Specifically, we first used Monte Carlo sampling to randomly generate a large number (10^8) of dust particles from the two lognormal distributions of AR and HWR. Second, for each of these generated particles, we used equations (5)–(7) and equation (4), respectively, to obtain its terminal velocity and that of its volume-equivalent spherical particle. Finally, for each dust particle, we calculated the reduction in terminal velocity (as $1-\frac{v_{asp}}{v_{sph}}$) and the enhancement of the gravitational settling lifetime (as $\frac{T_{asp}-T_{sph}}{T_{sph}} = \frac{v_{sph}}{v_{asp}} - 1$). Note that $T_{asp} \propto \frac{1}{v_{asp}}$ and $T_{sph} \propto \frac{1}{v_{sph}}$ are the gravitational settling lifetimes of aspherical dust and its volume-equivalent spherical dust, respectively.

We find that accounting for dust asphericity decreases gravitational settling speed by ~15% (Figure 4a). This value is larger than the <5% reduction in gravitational settling speed reported by Ginoux (2003) for dust <20 μm in diameter. Because Ginoux (2003) approximated dust as prolate spheroids (Figure S1b) with a median AR of 1.5, this study underestimated dust asphericity by overestimating dust height. As a result, Ginoux (2003) underestimated the reduction in gravitational settling speed due to particle asphericity.

We further find that the reduction in gravitational settling speed due to dust asphericity increases the lifetime with respect to gravitational settling by ~20% (Figure 4b). Because coarse dust is primarily removed from the atmosphere by gravitational settling (Mahowald et al., 2014), this finding helps explain why climate models generally underestimate the amount of coarse dust ($D > 5$ μm) in the atmosphere (Adebiyi et al., 2020). Specifically, measurements of dust size distributions have found that more coarse dust particles are present in the atmosphere than simulated in climate models (e.g., Ansmann et al., 2017; Ryder et al., 2018; van der Does et al., 2018). Several mechanisms have been proposed that could contribute to this modeled underestimation of coarse dust, including turbulent vertical mixing in dust layers (Gasteiger et al., 2017), electrostatic charging of dust (Harrison et al., 2018), and numerical diffusion (Ginoux, 2003). Although future work is needed to test whether accounting for dust asphericity indeed improves dust simulations in global models, our finding that dust asphericity results in a ~20% increase in dust lifetime indicates that dust asphericity also contributes to the underestimation of coarse dust in climate models.

5. Limitations of Methodology

Our methodology is subject to a few important limitations. First, we assume that AR and HWR are not correlated. This simplification is supported by Sakai et al. (2010), whose data show only a small correlation of 0.17 between AR and HWR for 1,941 dust particles. Second, our methodology is unable to account for several smaller systematic differences that exist between studies, due to, for instance, different software algorithms used in measuring particle dimensions (see supporting information Text S2). Third, we assume that dust aerosols are randomly oriented in the atmosphere in section 4, following Ginoux (2003) and Bagheri and Bonadonna (2016). However, especially larger dust particles could assume a preferential orientation that increases their drag (Ulanowski et al., 2007; Westbrook, 2008). This would reduce the terminal velocity of coarse dust more than we estimated and strengthen our conclusion that dust asphericity contributes to the underestimation of coarse dust by climate models. Fourth, we approximate dust as tri-axial ellipsoidal particles and do not consider the effect of dust surface roughness (Kalashnikova et al., 2005). As surface roughness leads to a greater surface area and therefore a larger drag force, this could also cause an

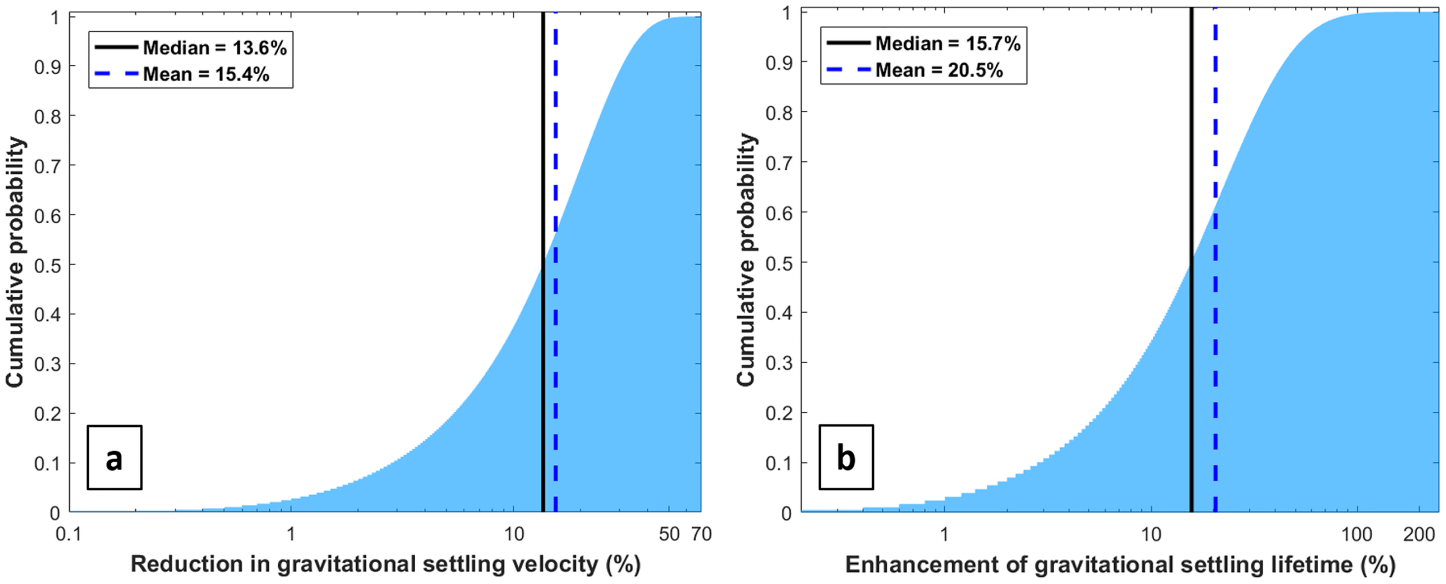

Figure 4. Probability distributions of (a) the reduction in gravitational settling velocity and (b) the enhancement of lifetime with respect to gravitational settling due to dust asphericity. Because deposition of dust with $D < 20$ μm occurs in the Stokes regime, the effect of asphericity on dust gravitational settling is independent of size.

underestimation of the reduction in terminal velocity. Finally, we use size-invariant globally-averaged medians and geometric standard deviations of AR and HWR and therefore neglect any dependence of the enhancement of gravitational settling lifetime on dust size and source region. As HWR may decrease with dust size (Figure 2c), we may overestimate the reduction in terminal velocity for fine dust and underestimate it for coarse dust.

6. Conclusions

Current climate models and remote sensing retrievals approximate dust aerosols as spherical or spheroidal particles and therefore assume that either all three or two of the three dimensions of dust aerosols are equal. Here, we showed that this assumption causes climate models and remote sensing retrievals to substantially underestimate dust asphericity. We showed this by compiling dozens of measurements of the AR and the HWR of dust aerosols across the globe. These compiled measurements indicate that North African dust becomes more aspherical during transport, most likely because of preferential settling of spherical particles. In contrast, Asian dust may become less aspherical during transport, possibly because of chemical processing. When combining all available measurements, our compilation shows that the largest dimension of dust aerosols is on average 5 times larger than the smallest dimension. Consequently, the assumption in climate models and remote sensing retrievals that at least two dimensions are equal causes an underestimation of dust asphericity by a factor of ~3–5.

This underestimation of dust asphericity could produce important errors in calculations of dust impacts on the Earth system. For instance, using the compiled globally-averaged shape distributions of AR and HWR, we find that accounting for dust asphericity increases dust lifetime with respect to gravitational settling by ~20%. This increased lifetime helps explain the underestimation of coarse dust transport by models (Ansmann et al., 2017; Huneeus et al., 2011).

The globally-averaged shape distributions of dust aerosols obtained in this paper can be used to inform more accurate calculations of dust impacts on the Earth system. This includes better estimates of dust lifetime, dust optics, and dust impacts on cloud and heterogeneous chemistry.

Acknowledgments
The authors thank the two anonymous reviewers for their constructive comments that helped to improve the manuscript. Y. H. acknowledges the support from the National Aeronautics and Space Administration (NASA) Grant 80NSSC19K1346, awarded under the Future Investigators in NASA Earth and Space Science and Technology (FINESST) program. J. F. K is funded by the National Science Foundation (NSF) Grants 1552519 and 1856389. K. K. is funded by Deutsche Forschungsgemeinschaft (DFG, German Research Foundation)—416816480. H. L. is funded by the Academy of Finland Grant 285421. A. A. is funded by the University of California President's Postdoctoral Fellowship. The authors further thank Kazuo Osada, Gholamhossein Bagheri, Gi Young Jeong, Paula Formenti, and Adriana Rocha-Lima for providing experimental data and thank Evan Variano, Ralph Kahn, Olga Kalashnikova, Aliaksandr Sinyuk, Marcelo Chamecki, and Robert Green for insightful discussions. Compiled dust shape data are listed in the supporting information Tables S2 and S3. Code scripts used in section 4 are available in a publicly accessible repository (https://doi.org/10.5281/zenodo.3633351).

References

Adebiyi, A. A., Kok, J. F., Wang, Y., Ito, A., Ridley, D. A., Nabat, P., & Zhao, C. (2020). Dust constraints from joint Observational-Modelling-experiMental analysis (DustCOMM): Comparison with measurements and model simulations. *Atmospheric Chemistry and Physics*, *20*(2), 829–863. https://doi.org/10.5194/acp-2019-484

Alexander, J. M., Grassian, V. H., Young, M. A., & Kleiber, P. D. (2015). Optical properties of selected components of mineral dust aerosol processed with organic acids and humic material. *Journal of Geophysical Research: Atmospheres*, *120*, 2437–2452. https://doi.org/10.1002/2014JD022782

Almeida-Prieto, S., Blanco-Méndez, J., & Otero-Espinar, F. J. (2007). Microscopic image analysis techniques for the morphological characterization of pharmaceutical particles: Influence of the software, and the factor algorithms used in the shape factor estimation. *European Journal of Pharmaceutics and Biopharmaceutics*, *67*(3), 766–776. https://doi.org/10.1016/j.ejpb.2007.04.001

Ansmann, A., Rittmeister, F., Engelmann, R., Basart, S., Jorba, O., Spyrou, C., et al. (2017). Profiling of Saharan dust from the Caribbean to western Africa—Part 2: Shipborne lidar measurements versus forecasts. *Atmospheric Chemistry and Physics*, *17*(24), 14,987–15,006. https://doi.org/10.5194/acp-17-14987-2017

Bagheri, G., & Bonadonna, C. (2016). On the drag of freely falling non-spherical particles. *Powder Technology*, *301*, 526–544. https://doi.org/10.1016/j.powtec.2016.06.015

Boucher, O., Randall, D., Artaxo, P., Bretherton, C., Feingold, G., Forster, P., et al. (2013). Clouds and aerosols. In T. F. Stocker, D. Qin, G.-K. Plattner, M. Tignor, S. K. Allen, J. Boschung, A. Nauels, Y. Xia, V. Bex, & P. M. Midgley (Eds.), *Climate Change 2013: The Physical Science Basis. Contribution of Working Group I to the Fifth Assessment Report of the Intergovernmental Panel on Climate Change*. Cambridge, United Kingdom and New York, NY: Cambridge University Press.

Burnett, R. T., Pope, C. A. III, Ezzati, M., Olives, C., Lim, S. S., Mehta, S., et al. (2014). An integrated risk function for estimating the global burden of disease attributable to ambient fine particulate matter exposure. *Environmental Health Perspectives*, *122*(4), 397–403. https://doi.org/10.1289/ehp.1307049

Chou, C., Formenti, P., Maille, M., Ausset, P., Helas, G., Harrison, M., & Osborne, S. (2008). Size distribution, shape, and composition of mineral dust aerosols collected during the African monsoon multidisciplinary analysis special observation period 0: Dust and biomass-burning experiment field campaign in Niger, January 2006. *Journal of Geophysical Research*, *113*, D00C10. https://doi.org/10.1029/2008JD009897

Coz, E., Gómez-Moreno, F. J., Pujadas, M., Casuccio, G. S., Lersch, T. L., & Artíñano, B. (2009). Individual particle characteristics of North African dust under different long-range transport scenarios. *Atmospheric Environment*, *43*(11), 1850–1863. https://doi.org/10.1016/j.atmosenv.2008.12.045

DeMott, P. J., Sassen, K., Poellot, M. R., Baumgardner, D., Rogers, D. C., Brooks, S. D., et al. (2003). African dust aerosols as atmospheric ice nuclei. *Geophysical Research Letters*, *30*(14), 1732. https://doi.org/10.1029/2003GL017410

Denjean, C., Caquineau, S., Desboeufs, K., Laurent, B., Maille, M., Quiñones Rosado, M., et al. (2015). Long-range transport across the Atlantic in summertime does not enhance the hygroscopicity of African mineral dust. *Geophysical Research Letters*, *42*, 7835–7843. https://doi.org/10.1002/2015GL065693

Dubovik, O., Sinyuk, A., Lapyonok, T., Holben, B. N., Mishchenko, M., Yang, P., et al. (2006). Application of spheroid models to account for aerosol particle nonsphericity in remote sensing of desert dust. *Journal of Geophysical Research*, *111*, D11208. https://doi.org/10.1029/2005JD006619

Formenti, P., Schütz, L., Balkanski, Y., Desboeufs, K., Ebert, M., Kandler, K., et al. (2011). Recent progress in understanding physical and chemical properties of African and Asian mineral dust. *Atmospheric Chemistry and Physics*, *11*(16), 8231–8256. https://doi.org/10.5194/acp-11-8231-2011

Gasteiger, J., Groß, S., Sauer, D., Haarig, M., Ansmann, A., & Weinzierl, B. (2017). Particle settling and vertical mixing in the Saharan Air Layer as seen from an integrated model, lidar, and in situ perspective. *Atmospheric Chemistry and Physics*, *17*(1), 297–311. https://doi.org/10.5194/acp-17-297-2017

Ginoux, P. (2003). Effects of nonsphericity on mineral dust modeling. *Journal of Geophysical Research*, *108*(D2), 4052. https://doi.org/10.1029/2002JD002516

Ginoux, P., Prospero, J. M., Gill, T. E., Hsu, N. C., & Zhao, M. (2012). Global-scale attribution of anthropogenic and natural dust sources and their emission rates based on MODIS Deep Blue aerosol products. *Reviews of Geophysics*, *50*, RG3005. https://doi.org/10.1029/2012RG000388

Harrison, R. G., Nicoll, K. A., Marlton, G. J., Ryder, C. L., & Bennett, A. J. (2018). Saharan dust plume charging observed over the UK. *Environmental Research Letters*, *13*(5), 1–9. https://doi.org/10.1088/1748-9326/aabcd9

Hinds, W. C. (1999). *Aerosol technology: Properties, behavior, and measurement of airborne particles* (2nd ed.). New York NY: Wiley-Interscience.

Hsu, N. C., Lee, J., Sayer, A. M., Kim, W., Bettenhausen, C., & Tsay, S.-C. (2019). VIIRS Deep blue aerosol products over land: Extending the EOS long-term aerosol data records. *Journal of Geophysical Research: Atmospheres*, *124*, 4026–4053. https://doi.org/10.1029/2018jd029688

Huang, Y., Kok, J. F., Martin, R. L., Swet, N., Katra, I., Gill, T. E., et al. (2019). Fine dust emissions from active sands at coastal Oceano Dunes, California. *Atmospheric Chemistry and Physics*, *19*(5), 2947–2964. https://doi.org/10.5194/acp-19-2947-2019

Huneeus, N., Schulz, M., Balkanski, Y., Griesfeller, J., Prospero, J., Kinne, S., et al. (2011). Global dust model intercomparison in AeroCom phase I. *Atmospheric Chemistry and Physics*, *11*(15), 7781–7816. https://doi.org/10.5194/acp-11-7781-2011

Jeong, G. Y., Park, M. Y., Kandler, K., Nousiainen, T., & Kemppinen, O. (2016). Mineralogical properties and internal structures of individual fine particles of Saharan dust. *Atmospheric Chemistry and Physics*, *16*(19), 12,397–12,410. https://doi.org/10.5194/acp-16-12397-2016

Jickells, T. D., An, Z. S., Andersen, K. K., Baker, A. R., Bergametti, G., Brooks, N., et al. (2005). Global Iron Connections Between Desert Dust, Ocean Biogeochemistry, and Climate. *Science*, *308*(5718), 67–71. https://doi.org/10.1126/science.1105959

Kalashnikova, O. V., & Kahn, R. (2006). Ability of multiangle remote sensing observations to identify and distinguish mineral dust types: 2. Sensitivity over dark water. *Journal of Geophysical Research*, *111*, D11207. https://doi.org/10.1029/2005JD006756

Kalashnikova, O. V., Kahn, R., Sokolik, I. N., & Li, W. H. (2005). Ability of multiangle remote sensing observations to identify and distinguish mineral dust types: Optical models and retrievals of optically thick plumes. *Journal of Geophysical Research*, *110*, D18S14. https://doi.org/10.1029/2004JD004550

Kandler, K., Benker, N., Bundke, U., Cuevas, E., Ebert, M., Knippertz, P., et al. (2007). Chemical composition and complex refractive index of Saharan Mineral Dust at Izaña, Tenerife (Spain) derived by electron microscopy. *Atmospheric Environment*, *41*(37), 8058–8074. https://doi.org/10.1016/j.atmosenv.2007.06.047

Kandler, K., Lieke, K., Benker, N., Emmel, C., Küpper, M., Müller-Ebert, D., et al. (2011). Electron microscopy of particles collected at Praia, Cape Verde, during the Saharan mineral dust experiment: Particle chemistry, shape, mixing state and complex refractive index. *Tellus Series B: Chemical and Physical Meteorology*, *63*(4), 475–496. https://doi.org/10.1111/j.1600-0889.2011.00550.x

Kandler, K., Schütz, L., Deutscher, C., Ebert, M., Hofmann, H., Jäckel, S., et al. (2009). Size distribution, mass concentration, chemical and mineralogical composition and derived optical parameters of the boundary layer aerosol at Tinfou, Morocco, during SAMUM 2006. *Tellus Series B: Chemical and Physical Meteorology*, *61*(1), 32–50. https://doi.org/10.1111/j.1600-0889.2008.00385.x

Klaver, A., Formenti, P., Caquineau, S., Chevaillier, S., Ausset, P., Calzolai, G., et al. (2011). Physico-chemical and optical properties of Sahelian and Saharan mineral dust: In situ measurements during the GERBILS campaign. *Quarterly Journal of the Royal Meteorological Society*, *137*(658), 1193–1210. https://doi.org/10.1002/qj.889

Kok, J. F., Parteli, E. J. R., Michaels, T. I., & Karam, D. B. (2012). The physics of wind-blown sand and dust. *Reports on Progress in Physics*, *75*(10), 106901 https://doi.org/10.1088/0034-4885/75/10/106901

Kok, J. F., Ridley, D. A., Zhou, Q., Miller, R. L., Zhao, C., Heald, C. L., et al. (2017). Smaller desert dust cooling effect estimated from analysis of dust size and abundance. *Nature Geoscience*, *10*(4), 274–278. https://doi.org/10.1038/ngeo2912

Laskina, O., Young, M. A., Kleiber, P. D., & Grassian, V. H. (2013). Infrared extinction spectroscopy and micro-Raman spectroscopy of select components of mineral dust mixed with organic compounds. *Journal of Geophysical Research: Atmospheres*, *118*, 6593–6606. https://doi.org/10.1002/jgrd.50494

Li, J., & Osada, K. (2007). Water-insoluble particles in spring snow at Mt. Tateyama, Japan: Characteristics of the shape factors and size distribution in relation with their origin and transportation. *Journal of the Meteorological Society of Japan. Ser. 2*, *85*(2), 137–149. https://doi.org/10.2151/jmsj.85.137

Lieke, K., Kandler, K., Scheuvens, D., Emmel, C., Glahn, C. V., Petzold, A., et al. (2011). Particle chemical properties in the vertical column based on aircraft observations in the vicinity of Cape Verde Islands. *Tellus Series B: Chemical and Physical Meteorology*, *63*(4), 497–511. https://doi.org/10.1111/j.1600-0889.2011.00553.x

Lindqvist, H., Jokinen, O., Kandler, K., Scheuvens, D., & Nousiainen, T. (2014). Single scattering by realistic, inhomogeneous mineral dust particles with stereogrammetric shapes. *Atmospheric Chemistry and Physics*, *14*(1), 143–157. https://doi.org/10.5194/acp-14-143-2014

Mahowald, N., Albani, S., Kok, J. F., Engelstaeder, S., Scanza, R., Ward, D. S., & Flanner, M. G. (2014). The size distribution of desert dust aerosols and its impact on the Earth system. *Aeolian Research*, *15*, 53–71. https://doi.org/10.1016/j.aeolia.2013.09.002

Mahowald, N. M., Ballantine, J. A., Feddema, J., & Ramankutty, N. (2007). Global trends in visibility: Implications for dust sources. *Atmospheric Chemistry and Physics*, *7*(12), 3309–3339. https://doi.org/10.5194/acp-7-3309-2007

Matsuki, A., Schwarzenboeck, A., Venzac, H., Laj, P., Crumeyrolle, S., & Gomes, L. (2010). Cloud processing of mineral dust: Direct comparison of cloud residual and clear sky particles during AMMA aircraft campaign in summer 2006. *Atmospheric Chemistry and Physics*, *10*(3), 1057–1069. https://doi.org/10.5194/acp-10-1057-2010

Nousiainen, T., & Kandler, K. (2015). Light scattering by atmospheric mineral dust particles. *Light Scattering Reviews*, *9*, 3–52.

Okada, K., Heintzenberg, J., Kai, K., & Qin, Y. (2001). Shape of atmospheric mineral particles collected in three Chinese arid-regions. *Geophysical Research Letters*, *28*(16), 3123–3126. https://doi.org/10.1029/2000GL012798

Okada, K., Kobayashi, A., Iwasaka, Y., Naruse, H., Tanaka, T., & Nemoto, O. (1987). Features of individual Asian dust-storm particles collected at Nagoya, Japan. *Journal of the Meteorological Society of Japan. Ser. 2*, *65*(3), 515–521. https://doi.org/10.2151/jmsj1965.65.3_515

Osada, K. (2013). Water soluble fraction of Asian dust particles. *Atmospheric Research*, *124*, 101–108. https://doi.org/10.1016/j.atmosres.2013.01.001

Pérez, C., Nickovic, S., Pejanovic, G., Baldasano, J. M., & Özsoy, E. (2006). Interactive dust-radiation modeling: A step to improve weather forecasts. *Journal of Geophysical Research*, *111*, D16206. https://doi.org/10.1029/2005JD006717

Reid, E. A., Reid, J. S., Meier, M. M., Dunlap, M. R., Cliff, S. S., Broumas, A., et al. (2003). Characterization of African dust transported to Puerto Rico by individual particle and size segregated bulk analysis. *Journal of Geophysical Research*, *108*(D19), 8591. https://doi.org/10.1029/2002JD002935

Reid, J. S., Jonsson, H. H., Maring, H. B., Smirnov, A., Savoie, D. L., Cliff, S. S., et al. (2003). Comparison of size and morphological measurements of coarse mode dust particles from Africa. *Journal of Geophysical Research*, *108*(D19), 8593. https://doi.org/10.1029/2002JD002485

Rocha-Lima, A., Martins, J. V., Remer, L. A., Todd, M., Marsham, J. H., Engelstaedter, S., et al. (2018). A detailed characterization of the Saharan dust collected during the Fennec campaign in 2011: In situ ground-based and laboratory measurements. *Atmospheric Chemistry and Physics*, *18*(2), 1023–1043. https://doi.org/10.5194/acp-18-1023-2018

Ryder, C. L., Marenco, F., Brooke, J. K., Estelles, V., Cotton, R., Formenti, P., et al. (2018). Coarse-mode mineral dust size distributions, composition and optical properties from AER-D aircraft measurements over the tropical eastern Atlantic. *Atmospheric Chemistry and Physics*, *18*(23), 17225–17257. https://doi.org/10.5194/acp-18-17225-2018

Sakai, T., Nagai, T., Zaizen, Y., & Mano, Y. (2010). Backscattering linear depolarization ratio measurements of mineral, sea-salt, and ammonium sulfate particles simulated in a laboratory chamber. *Applied Optics*, *49*(23), 4441–4449. https://doi.org/10.1364/AO.49.004441

Scheuvens, D., Kandler, K., Küpper, M., Lieke, K., Zorn, S. R., Ebert, M., et al. (2011). Individual-particle analysis of airborne dust samples collected over Morocco in 2006 during SAMUM 1. *Tellus Series B: Chemical and Physical Meteorology*, *63*(4), 512–530. https://doi.org/10.1111/j.1600-0889.2011.00554.x

Ulanowski, Z., Bailey, J., Lucas, P. W., Hough, J. H., & Hirst, E. (2007). Alignment of atmospheric mineral dust due to electric field. *Atmospheric Chemistry and Physics*, *7*(24), 6161–6173. https://doi.org/10.5194/acp-7-6161-2007

Usher, C. R., Al-Hosney, H., Carlos-Cuellar, S., & Grassian, V. H. (2002). A laboratory study of the heterogeneous uptake and oxidation of sulfur dioxide on mineral dust particles. *Journal of Geophysical Research*, *107*(D23), 4713. https://doi.org/10.1029/2002JD002051

van der Does, M., Knippertz, P., Zschenderlein, P., Harrison, R. G., & Stuut, J.-B. W. (2018). The mysterious long-range transport of giant mineral dust particles. *Science Advances*, *4*(12), 1–8. https://doi.org/10.1126/sciadv.aau2768

Wagner, R., Ajtai, T., Kandler, K., Lieke, K., Linke, C., Müller, T., et al. (2012). Complex refractive indices of Saharan dust samples at visible and near UV wavelengths: A laboratory study. *Atmospheric Chemistry and Physics*, *12*(5), 2491–2512. https://doi.org/10.5194/acp-12-2491-2012

Westbrook, C. D. (2008). The fall speeds of sub-100 μm ice crystals. *Quarterly Journal of the Royal Meteorological Society*, *134*(634), 1243–1251. https://doi.org/10.1002/qj.290

Woodward, X., Kostinski, A., China, S., Mazzoleni, C., & Cantrell, W. (2015). Characterization of dust particles' 3D shape and roughness with nanometer resolution. *Aerosol Science and Technology*, *49*(4), 229–238. https://doi.org/10.1080/02786826.2015.1017550

Yang, W., Marshak, A., Kostinski, A. B., & Várnai, T. (2013). Shape-induced gravitational sorting of Saharan dust during transatlantic voyage: Evidence from CALIOP lidar depolarization measurements. *Geophysical Research Letters*, *40*, 3281–3286. https://doi.org/10.1002/grl.50603

Zhang, D. (2008). Effect of sea salt on dust settling to the ocean. *Tellus Series B: Chemical and Physical Meteorology*, *60*(4), 641–646. https://doi.org/10.1111/j.1600-0889.2008.00358.x

References From the Supporting Information

Nishikawa, M., Hao, Q., & Morita, M. (2000). Preparation and evaluation of certified reference materials for Asian mineral dust. *Global Environmental Research*, *4*, 103–113.

Schütz, L., & Sebert, M. (1987). Mineral aerosols and source identification. *Journal of Aerosol Science*, *18*(1), 1–10. https://doi.org/10.1016/0021-8502(87)90002-4